Periodic Trends in the Binding of Metal Ions to Pyridine Studied by Threshold Collision-Induced Dissociation and Density Functional Theory

M. T. Rodgers,* J. R. Stanley, and R. Amunugama

Contribution from the Department of Chemistry, Wayne State University, Detroit, Michigan 48202

Received July 28, 2000

Abstract: Threshold collision-induced dissociation of M^+(pyridine) with xenon is studied using guided ion beam mass spectrometry. M^+ include the following metal ions: Mg^+, Al^+, Sc^+, Ti^+, V^+, Cr^+, Mn^+, Fe^+, Co^+, Ni^+, Cu^+, and Zn^+. In all cases, the primary product corresponds to endothermic loss of the intact pyridine molecule, with minor production of MXe^+ formed by ligand exchange. In the Cr^+(pyridine) system, an additional minor reaction pathway involving a ring-opening reaction with small neutral molecule loss is also observed. The cross-section thresholds are interpreted to yield 0 and 298 K bond dissociation energies for M^+−pyridine after accounting for the effects of multiple ion−molecule collisions, internal energy of the reactant ions, and dissociation lifetimes. Density functional calculations at the B3LYP/6-31G(d,p) level of theory are used to determine the structures of these complexes and provide molecular constants necessary for the thermodynamic analysis of the experimental data. Theoretical bond dissociation energies at this level of theory are unreliable as even the trends in the calculated values do not parallel measured values. Measured M^+−pyridine bond dissociation energies compare favorably to the four values previously determined by kinetic method or photodissociation experiments.

Introduction

Metal ions are involved in all biological processes that nucleic acids participate in. The effects of binding a metal ion to a nucleic acid vary from stabilization of the three-dimensional structure to transcription failure and even cell death. This variation in effect results from several possible sites where the metal ion can interact with the nucleic acid: at the phosphate backbone, at the sugar moiety, or at the base. The presence, identity, and location of metal ions strongly influence the conformation of a nucleic acid, which in turn controls the activity of nucleic acids. Nonspecific binding of metal ions to the phosphate backbone gives rise to stabilization of the double helix through neutralization of the negative charges residing on the phosphate backbone. Binding of a metal ion to the base also neutralizes the negative phosphate charge, but can interfere with hydrogen bonding and stacking interactions between bases. Such metal−base interactions may destabilize the helix. Erroneous pairing and subsequent transcription errors may occur if the metal ion interferes with base−base interactions. The course of genetic information transfer may be altered by metal ion−nucleic acid interactions.[1]

Metal ions that are "hard" and have a low tendency to form covalent bonds tend to bind to the phosphate backbone. The alkali metal ions and Mg^{2+} behave in this manner.[1] Other metal ions, such as transition metal ions, have a greater likelihood to form covalent bonds and are softer than the alkali metal ions. Competition between the phosphate backbone and the bases for binding of transition metal ions is therefore much more likely. An understanding of the interactions of various metals with nucleic acids is essential to understand the role and effects of metal ions in their biological activity.

In recent work, we have developed methods to allow the application of quantitative threshold collision-induced dissociation methods to obtain accurate thermodynamic information on increasingly large systems.[2−8] One of the driving forces behind these developments is our interest in applying such techniques to systems having biological relevance. In addition, we seek to perform accurate thermochemical measurements that provide absolute anchors for metal cation affinity scales over an ever-broadening range of energies. In the present paper, we examine the interactions of pyridine, the simplest six-membered heterocycle-containing nitrogen, with various metal ions. The structure of pyridine is shown in Figure 1 along with its calculated[9] and measured[10] dipole moments, and estimated polarizability.[11] Pyridine was chosen as a simple model of noncovalent interaction with metal ions for a wide variety of nitrogen-containing heterocycles of biological importance, and of particular interest, the nucleic acid bases.

(1) Eichhorn, G. L. *Adv. Inorg. Biochem.* **1981**, *2*, 1.

(2) Rodgers, M. T.; Armentrout, P. B. *J. Phys. Chem. A* **1997**, *101*, 1238.
(3) Rodgers, M. T.; Armentrout, P. B. *J. Phys. Chem. A* **1997**, *101*, 2614.
(4) Rodgers, M. T.; Ervin, K. M.; Armentrout, P. B. *J. Chem. Phys.* **1997**, *106*, 4499.
(5) Rodgers, M. T.; Armentrout, P. B. *Int. J. Mass Spectrom.* **1999**, *185/186/187*, 359.
(6) Rodgers, M. T.; Armentrout, P. B. *J. Phys. Chem. A* **1999**, *103*, 4955.
(7) Armentrout, P. B.; Rodgers, M. T. *J. Phys. Chem. A* **2000**, *104*, 2238.
(8) Amunugama, R.; Rodgers, M. T. *Int. J. Mass Spectrom.* **2000**, *195/196*, 439.
(9) Mátyus, P.; Fugi, K.; Tanaka, K. *Tetrahedron* **1994**, *50*, 2405.
(10) (a) Boulton, A. J.; McKillop, A. *Comprehensive Heterocyclic Chemistry*; Katritzky, A. R., Rees, C. W., Eds.; Pergamon Press: Oxford; 1984, Vol. 2, p 7. (b) Tisler, M.; Stanovnik, B. *Comprehensive Heterocyclic Chemistry*; Katritzky, A. R., Rees, C. W., Eds.; Pergamon Press: Oxford; 1984, Vol. 3, pp 2−3. (c) Porter, A. E. A. *Comprehensive Heterocyclic Chemistry*; Katritzky, A. R., Rees, C. W., Eds.; Pergamon Press: Oxford; 1984, Vol. 3, pp 158−162.
(11) Miller, K. J. *J. Am. Chem. Soc.* **1990**, *112*, 8533.

10.1021/ja0027923 CCC: $19.00
Published on Web 10/21/2000

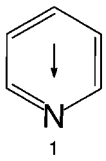

1

pyridine

2.22 D (2.20 D)

9.51 Å3

Figure 1. Structure of the pyridine molecule. The dipole moment is shown as an arrow. Values for the dipole moment are taken from theory (ref 19) and experiment, listed in parentheses (ref 20). The estimated polarizability is also shown (ref 21).

Pyridine is one of the most abundant and best known of the aromatic heterocycles. Compounds containing the pyridine ring are widely distributed in nature, principally as enzymes and alkaloids. Others are obtained by degradation of complex natural materials such as coal, shale, and various alkaloids. Coal is the only commercially important source of pyridine compounds.[12] Of the naturally occurring pyridine compounds, those having the greatest biochemical importance are Vitamin B_6 and two coenzymes containing nicotinamide: nicotinamide adenine dinucleotide (NAD^+) and nicotinamide adenine dinucleotide phosphate ($NADP^+$).[13] NAD^+ and $NADP^+$ function as coenzymes of more than 200 oxidoreductases, collectively called pyridine-linked dehydrogenases, which are known to function in different aspects of metabolism.[14] Pyridine enzymes have been found in the tissues of all plants and animals examined thus far, and are derived from either nicotinic acid or Vitamin B_6.[12] Pyridine is also the building block of many pharmaceuticals with functionalities that range from anti-tubercular compounds, antiviral and antitumor agents, central nervous system stimulants, diagnostic agents, analgesics, antiinflammatory agents, and antihistamines.[15,16]

In the present study, we use guided ion beam mass spectrometry to collisionally excite complexes of M^+ bound to pyridine, where $M^+ = Mg^+$, Al^+, Sc^+, Ti^+, V^+, Cr^+, Mn^+, Fe^+, Co^+, Ni^+, Cu^+, and Zn^+. The kinetic energy-dependent cross sections for the collision-induced dissociation (CID) processes are analyzed using methods developed previously.[4] The analysis explicitly includes the effects of the internal and translational energy distributions of the reactants, multiple collisions, and the lifetime for dissociation. We derive metal cation−pyridine bond dissociation energies (BDEs) for all of the complexes, and compare these results to literature values,[17−19] and to ab initio and density functional calculations performed here and in the literature.[8,9,19−22]

Experimental Section

General Procedures. Cross sections for CID of M^+(pyridine), where $M^+ = Mg^+$, Al^+, Sc^+, Ti^+, V^+, Cr^+, Mn^+, Fe^+, Co^+, Ni^+, Cu^+, and Zn^+, are measured using a guided ion beam mass spectrometer that has been described in detail previously.[23,24] The metal−ligand complexes are generated as described below. The ions are extracted from the source, accelerated, and focused into a magnetic sector momentum analyzer for mass analysis. Mass-selected ions are decelerated to a desired kinetic energy and focused into an octopole ion guide, which traps the ions in the radial direction.[25] The octopole passes through a static gas cell containing xenon, used as the collision gas, for reasons described elsewhere.[26−28] Low gas pressures in the cell (typically 0.04 to 0.20 mTorr) are used to ensure that multiple ion−molecule collisions are improbable. Product and unreacted beam ions drift to the end of the octopole where they are focused into a quadrupole mass filter for mass analysis and subsequently detected with a secondary electron scintillation detector and standard pulse counting techniques.

Ion intensities are converted to absolute cross sections as described previously.[23] Absolute uncertainties in cross section magnitudes are estimated to be ±20%, which are largely the result of errors in the pressure measurement and the length of the interaction region. Relative uncertainties are approximately ±5%.

Ion kinetic energies in the laboratory frame, E_{lab}, are converted to energies in the center of mass frame, E_{CM}, using the formula $E_{CM} = E_{lab}m/(m+M)$, where M and m are the masses of the ionic and neutral reactants, respectively. All energies reported below are in the CM frame unless otherwise noted. The absolute zero and distribution of the ion kinetic energies are determined using the octopole ion guide as a retarding potential analyzer as previously described.[23] The distribution of ion kinetic energies is nearly Gaussian with a fwhm typically between 0.2 and 0.4 eV (lab) for these experiments. The uncertainty in the absolute energy scale is ±0.05 eV (lab).

Even when the pressure of the reactant neutral is low, it has previously been demonstrated that the effects of multiple collisions can significantly influence the shape of CID cross sections.[29] Because the presence and magnitude of these pressure effects is difficult to predict, we have performed pressure-dependent studies of all cross-sections examined here. In the present systems, we observe small cross sections at low energies that have an obvious dependence upon pressure. We attribute this to multiple energizing collisions that lead to an enhanced probability of dissociation below threshold as a result of the longer residence time of these slower moving ions. Data free from pressure effects are obtained by extrapolating to zero reactant pressure, as described previously.[29] Thus, results reported below are due to single bimolecular encounters.

Ion Source. The M^+(pyridine) complexes are formed in a 1 m long flow tube[24,30] operating at a pressure of 0.7−0.8 Torr with a helium flow rate of approximately 600 sccm. Metal ions are generated in a continuous dc discharge by argon ion sputtering of a cathode, made from the metal of interest. Operating conditions of the discharge are 0.8−2.3 kV and 5−25 mA in a flow of roughly 10% argon in helium for the experiments performed here. The M^+(pyridine) complexes are

(12) Brody, F.; Ruby, P. R. In *Heterocyclic Compounds, Pyridine and Derivatives*; Klingsberg, E., Ed.; Interscience Publishers: New York, 1960; Part I, p 99.
(13) Acheson, R. M. *An Introduction to the Chemistry of Heterocyclic Compounds*; Interscience Publishers: John Wiley and Sons: New York, 1967; p 188.
(14) Lehninger, A. L. *Biochemistry*, 2nd ed.; Worth Publishers: New York, 1975.
(15) Coutts, R. T.; Casy, A. F. In *Pyridine and Its Derivatives*; Abramovitch, R. A., Ed.; John Wiley & Sons: New York, 1975; Suppl. Part 4, p 445.
(16) Gilchrist, T. L. *Heterocyclic Chemistry*, 3rd ed.; Longman Singapore Publishers Inc., Singapore, 1997; p 125.
(17) Ma, S.; Wong, P.; Yang, S. S.; Cooks, R. G. *J. Am. Chem. Soc.* **1996**, *118*, 6010.
(18) Wong, P. S. H.; Ma, S.; Wang, F.; Cooks, R. G. *J. Organomet. Chem.* **1997**, *539*, 131.
(19) Yang, Y.-S.; Hsu, W.-Y.; Lee, H.-F.; Huang, Y.-C.; Yeh, C.-S.; Hu, C.-H. *J. Phys. Chem. A* **1999**, *103*, 11287.
(20) Mó, O.; de Paz, J. L. G.; Yáñez, M. J. *Mol. Struct. (THEOCHEM)* **1987**, *150*, 135.
(21) Sanz, J. F.; Anguiano, J.; Vilarrasa, J. *J. Comput. Chem.* **1988**, *9*, 784.
(22) Stöckigt, D. *Organometallics* **1999**, *18*, 1050.
(23) Ervin, K. M.; Armentrout, P. B. *J. Chem. Phys.* **1985**, *83*, 166.
(24) Schultz, R. H.; Armentrout, P. B. *Int. J. Mass Spectrom. Ion Processes* **1991**, *107*, 29.
(25) Teloy, E.; Gerlich, D. *Chem. Phys.* **1974**, *4*, 417. Gerlich, D., Diplomarbeit, University of Freiburg, Federal Republic of Germany, 1971. Gerlich, D. In *State-Selected and State-to-State Ion−Molecule Reaction Dynamics, Part I, Experiment;* Ng, C.-Y., Baer, M., Eds.: *Adv. Chem. Phys.* **1992**, *82*, 1.
(26) Dalleska, N. F.; Honma, K.; Armentrout, P. B. *J. Am. Chem. Soc.* **1993**, *115*, 12125.
(27) Aristov, N.; Armentrout, P. B. *J. Phys. Chem.* **1986**, *90*, 5135.
(28) Hales, D. A.; Armentrout, P. B. *J. Cluster Sci.* **1990**, *1*, 127.
(29) Dalleska, N. F.; Honma, K.; Sunderlin, L. S.; Armentrout, P. B. *J. Am. Chem. Soc.* **1994**, *116*, 3519.
(30) Schultz, R. H.; Crellin, K. C.; Armentrout, P. B. *J. Am. Chem. Soc.* **1991**, *113*, 8590.

formed by associative reactions of the metal ion with the neutral pyridine, which is introduced into the flow 50 cm downstream from the dc discharge. The flow conditions used in this ion source provide in excess of 10^4 collisions between an ion and the buffer gas, which should thermalize the ions both vibrationally and rotationally. In our analysis of the data, we assume that the ions produced in this source are in their ground electronic states and that the internal energy of the M^+(pyridine) complexes is well described by a Maxwell−Boltzmann distribution of ro-vibrational states at 300 K. Previous work has shown that these assumptions are generally valid.[26,29−33]

Thermochemical Analysis. The threshold regions of the reaction cross sections are modeled using the equation

$$\sigma(E) = \sigma_0 \sum_i g_i (E + E_i - E_0)^n / E \qquad (1)$$

where σ_0 is an energy-independent scaling factor, E is the relative translational energy of the reactants, E_0 is the threshold for reaction of the ground electronic and ro-vibrational state, and n is an adjustable parameter. The summation is over the ro-vibrational states of the reactant ions, i, where E_i is the excitation energy of each state and g_i is the population of those states ($\sum g_i = 1$). The populations of excited ro-vibrational levels are not negligible even at 300 K as a result of the many low-frequency modes present in these ions. The relative reactivity of all ro-vibrational states, as reflected by σ_0 and n, is assumed to be equivalent.

To obtain model structures, vibrational frequencies, and energetics for the neutral and metalated pyridine, density functional theory calculations were performed using Gaussian 98.[34] Geometry optimizations were performed at the B3LYP/6-31G(d,p) level. Vibrational analyses of the geometry-optimized structures were performed to determine the vibrational frequencies and rotational constants of the molecules. When used to model the data or to calculate thermal energy corrections, the B3LYP/6-31G(d,p) vibrational frequencies are scaled by a factor of 0.9613.[35,36] The scaled vibrational frequencies thus obtained for the 12 systems studied are available as Supporting Information and listed in Table S1, while Table S2 lists the rotational constants.

The Beyer−Swinehart algorithm[37] is used to evaluate the density of the ro-vibrational states and the relative populations g_i are calculated by an appropriate Maxwell−Boltzmann distribution at the 300 K temperature appropriate for the reactants. The average vibrational energy at 298 K of the metal ion-bound pyridine is also given in Table S1. We have estimated the sensitivity of our analysis to the deviations from the true frequencies by scaling the calculated frequencies to encompass the range of average valence coordinate scale factors needed to bring calculated frequencies into agreement with experimentally determined frequencies found by Pople et al.[38] Thus, the originally calculated vibrational frequencies were increased and decreased by 10%. The corresponding change in the average vibrational energy is taken to be an estimate of one standard deviation of the uncertainty in vibrational energy (Table S1) and is included in the uncertainties, reported as one standard deviation, listed with the E_0 values.

We also consider the possibility that collisionally activated complex ions do not dissociate on the time scale of our experiment (about 10^{-4} s) by including statistical theories for unimolecular dissociation into eq 1 as described in detail elsewhere.[4,31] This requires sets of ro-vibrational frequencies appropriate for the energized molecules and the transition states (TSs) leading to dissociation. The former are given in Tables S1 and S2, while we assume that the TSs are loose and product-like because the interaction between the metal ion and the pyridine ligand is largely electrostatic. In this case, the TS vibrations used are the frequencies corresponding to the products, which are also found in Table S1. The transitional frequencies, those that become rotations of the completely dissociated products, are treated as rotors, a treatment that corresponds to a phase space limit (PSL) and is described in detail elsewhere.[4] For the M^+(pyridine) complexes, the two transitional mode rotors have rotational constants equal to those of the neutral pyridine product with axes perpendicular to the reaction coordinate. These are listed in Table S2. The external rotations of the energized molecule and TS are also included in the modeling of the CID data. The external rotational constants of the TS are determined by assuming that the TS occurs at the centrifugal barrier for interaction of M^+ with the neutral pyridine ligand, calculated variationally as outlined elsewhere.[4] The 2-D external rotations are treated adiabatically but with centrifugal effects included, consistent with the discussion of Waage and Rabinovitch.[39] In the present work, the adiabatic 2-D rotational energy is treated using a statistical distribution with explicit summation over the possible values of the rotational quantum number, as described in detail elsewhere.[3]

The model represented by eq 1 is expected to be appropriate for translationally driven reactions[40] and has been found to reproduce reaction cross sections well in a number of previous studies of both atom−diatom and polyatomic reactions,[41,42] including CID processes.[2,3,26,29−31,43−45] The model is convoluted with the kinetic energy distributions of both reactants, and a nonlinear least-squares analysis of the data is performed to give optimized values for the parameters σ_0, E_0, and n. The error associated with the measurement of E_0 is estimated from the range of threshold values determined for different data sets, variations associated with uncertainties in the vibrational frequencies, and the error in the absolute energy scale, 0.05 eV (lab). For analyses that include the RRKM lifetime effect, the uncertainties in the reported E_0 values also include the effects of increasing and decreasing the time assumed available for dissociation (10^{-4} s) by a factor of 2.

Equation 1 explicitly includes the internal energy of the ion, E_i. All energy available is treated statistically, which should be a reasonable assumption because the internal (rotational and vibrational) energy of the reactants is redistributed throughout the ion upon impact with the collision gas. The threshold for dissociation is by definition the minimum energy required leading to dissociation and thus corresponds to formation of products with no internal excitation. The assumption that products formed at threshold have an internal temperature of 0 K has been tested for several systems.[2,3,26,29−31] It has also been shown that treating all energy of the ion (vibrational, rotational, and transla-

(31) Khan, F. A.; Clemmer, D. C.; Schultz, R. H.; Armentrout, P. B. *J. Phys. Chem*. **1993**, *97*, 7978.
(32) Schultz, R. H.; Armentrout, P. B. *J. Chem. Phys*. **1992**, *96*, 1046.
(33) Fisher, E. R.; Kickel, B. L.; Armentrout, P. B. *J. Phys. Chem*. **1993**, *97*, 10204.
(34) Gaussian 98, Revision A.7, Frisch, M. J.; Trucks, G. W.; Schlegel, H. B.; Scuseria, G. E.; Robb, M. A.; Cheeseman, J. R.; Zakrzewski, V. G.; Montgomery, J. A., Jr.; Stratmann, R. E.; Burant, J. C.; Dapprich, S.; Millam, J. M.; Daniels, A. D.; Kudin, K. N.; Strain, M. C.; Farkas, O.; Tomasi, J.; Barone, V.; Cossi, M.; Cammi, R.; Mennucci, B.; Pomelli, C.; Adamo, C.; Clifford, S.; Ochterski, J.; Petersson, G. A.; Ayala, P. Y.; Cui, Q.; Morokuma, K.; Malick, D. K.; Rabuck, A. D.; Raghavachari, K.; Foresman, J. B.; Cioslowski, J.; Ortiz, J. V.; Stefanov, B. B.; Liu, G.; Liashenko, A.; Piskorz, P.; Komaromi, I.; Gomperts, R.; Martin, R. L.; Fox, D. J.; Keith, T.; Al-Laham, M. A.; Peng, C. Y.; Nanayakkara, A.; Gonzalez, C.; Challacombe, M.; Gill, P. M. W.; Johnson, B.; Chen, W.; Wong, M. W.; Andres, J. L.; Gonzales, C.; Head-Gordon, M.; Replogle, E. S.; Pople, J. A. Gaussian, Inc.: Pittsburgh, PA, 1998.
(35) Guo, B. C.; Conklin, B. J.; Castleman, A. W. *J. Am Chem. Soc*. **1989**, *111*, 6506.
(36) Foresman, J. B.; Frisch, Æ. *Exploring Chemistry with Electronic Structure Methods*, 2nd ed.; Gaussian: Pittsburgh, 1996.
(37) Beyer, T. S.; Swinehart, D. F. *Comm. Assoc. Comput. Machines* **1973**, *16*, 379. Stein, S. E.; Rabinovitch, B. S. *J. Chem. Phys*. **1973**, *58*, 2438. Stein, S. E.; Rabinovitch, B. S. *Chem. Phys. Lett*. **1977**, *49*, 1883.
(38) Pople, J. A.; Schlegel, H. B.; Raghavachari, K.; DeFrees, D. J.; Binkley, J. F.; Frisch, M. J.; Whitesides, R. F.; Hout, R. F.; Hehre, W. J. *Int. J. Quantum Chem. Symp*. **1981**, *15* 269. DeFrees, D. J.; McLean, A. D. *J. Chem. Phys*. **1985**, *82*, 333.
(39) Waage, E. V.; Rabinovitch, B. S. *Chem. Rev*. **1970**, *70*, 377.
(40) Chesnavich, W. J.; Bowers, M. T. *J. Phys. Chem*. **1979**, *83*, 900.
(41) Armentrout, P. B. In *Advances in Gas-Phase Ion Chemistry*; Adams, N. G., Babcock, L. M., Eds.; JAI: Greenwich, 1992; Vol. 1, pp 83−119.
(42) See, for example: Sunderlin, L. S.; Armentrout, P. B. *Int. J. Mass Spectrom. Ion Processes* **1989**, *94*, 149.
(43) More, M. B.; Glendening, E. D.; Ray, D.; Feller, D.; Armentrout, P. B. *J. Phys. Chem.* **1996**, *100*, 1605.
(44) Ray, D.; Feller, D.; More, M. B.; Glendening, E. D.; Armentrout, P. B. *J. Phys. Chem.* **1996**, *100*, 16116.
(45) Meyer, F.; Khan, F. A.; Armentrout, P. B. *J. Am. Chem. Soc*. **1995**, *117*, 9740.
(46) See, for example, Figure 1 in ref 26.

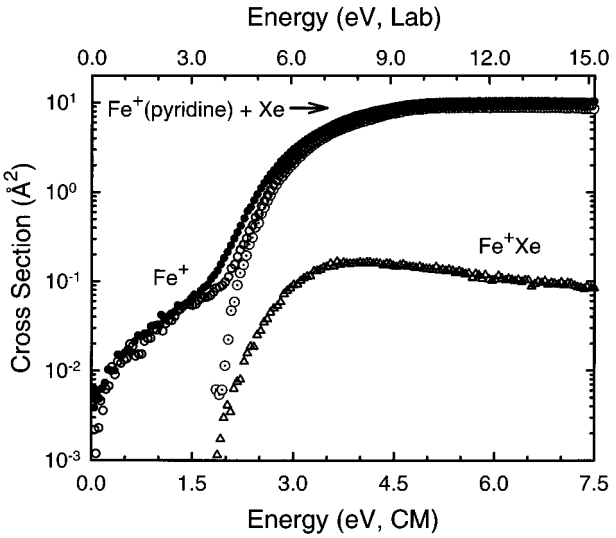

Figure 2. Cross sections for the collision-induced dissociation of the Fe^+(pyridine) complex with Xe as a function of the center-of-mass frame collision energy (lower *x*-axis) and laboratory frame (upper *x*-axis). Data for the Fe^+ product channel are shown for a Xe pressure of ~0.2 mTorr (●), extrapolated to zero (○), and after subtraction of the low-energy feature (⊙). The cross section for the ligand exchange process to form M + Xe is also shown (△).

tional) as capable of coupling into the dissociation coordinate leads to reasonable thermochemistry. The threshold energies for dissociation reactions determined by analysis with eq 1 are converted to 0 K bond energies by assuming that E_0 represents the energy difference between reactants and products at 0 K.[46] This assumption requires that there are no activation barriers in excess of the endothermicity of dissociation. This is generally true for ion−molecule reactions[41] and should be valid for the simple heterolytic bond fission reactions examined here.[47]

Results

Cross Sections for Collision-Induced Dissociation. Experimental cross sections were obtained for the interaction of Xe with 12 M^+(pyridine) complexes, where $M^+ = Mg^+$, Al^+, Sc^+, Ti^+, V^+, Cr^+, Mn^+, Fe^+, Co^+, Ni^+, Cu^+, and Zn^+. Figure 2 shows representative data for the Fe^+(pyridine) complex. The most favorable process for all complexes is the loss of the intact pyridine molecule in the collision-induced dissociation reactions 2.

$$M^+(\text{pyridine}) + Xe \rightarrow M^+ + \text{pyridine} + Xe \qquad (2)$$

For all metal ions except Cr^+, the only other product that is observed in the CID reactions is the result of a ligand exchange process to form MXe^+. (For Cr^+(pyridine), a product with a mass consistent with either CrH^+ or $C_4H_5^+$ was also generated, the former being more likely than cleaving the ring to form CrCN.) The cross sections for the MXe^+ products are approximately 1 to 2 orders of magnitude smaller than those of the primary dissociation product, M^+, and the thresholds are slightly lower (by the M^+−Xe binding energy). As little systematic information can be gleaned from these products, they will not be discussed further. However, it is conceivable that this ligand exchange process might cause a competitive shift in the observed thresholds. Within the quoted experimental errors, we do not believe such competition is likely to affect our threshold measurements in any of these systems for several reasons that have been detailed elsewhere.[48]

(47) Armentrout, P. B.; Simons, J. *J. Am. Chem. Soc.* **1992**, *114*, 8627.

Table 1. Modeling Parameters of Eq 1 and Entropies of Activation at 1000 K of M^+(pyridine)[a]

M^+	σ_0[b]	n[b]	E_0[c] (eV)	E_0(PSL) (eV)	kinetic shift (eV)	$\Delta S^{\ddagger}$(PSL) (J mol^{-1} K^{-1})
Mg^+	9.3(0.8)	1.5(0.1)	2.23(0.05)	2.07(0.07)	0.16	32(2)
Al^+	9.5(1.7)	1.5(0.1)	2.07(0.11)	1.97(0.11)	0.10	32(3)
Sc^+	8.7(0.8)	1.2(0.1)	2.63(0.09)	2.40(0.11)	0.23	32(2)
Ti^+	5.8(0.4)	1.3(0.1)	2.45(0.07)	2.25(0.10)	0.20	32(3)
V^+	8.6(3.1)	1.2(0.2)	2.42(0.16)	2.27(0.14)	0.15	40(2)
Cr^+	3.7(0.3)	1.2(0.1)	2.16(0.15)	2.04(0.12)	0.12	36(2)
Mn^+	12.2(2.3)	1.6(0.2)	1.98(0.10)	1.88(0.09)	0.10	30(3)
Fe^+	13.4(0.6)	1.3(0.1)	2.53(0.23)	2.32(0.09)	0.21	35(3)
Co^+	8.6(1.2)	1.4(0.2)	2.85(0.11)	2.56(0.13)	0.29	38(3)
Ni^+	5.4(1.4)	1.5(0.2)	2.94(0.18)	2.64(0.16)	0.30	40(3)
Cu^+	4.8(0.2)	1.2(0.1)	2.83(0.06)	2.55(0.10)	0.28	40(3)
Zn^+	4.3(0.1)	0.9(0.1)	2.87(0.03)	2.56(0.07)	0.31	34(2)

[a] Uncertainties are listed in parentheses. [b] Average values for loose PSL transition state. [c] No RRKM analysis.

As discussed above, the nonzero cross sections observed in the M^+ product data at the lowest energies are generally a consequence of multiple collisions and disappear when the data are extrapolated to zero pressure of the Xe reactant. In the present work, this is only true for the Cr^+ and Zn^+ systems. Even after pressure extrapolation, the remainder of the systems examined here continue to show a nonzero cross section at kinetic energies below the CID thresholds. This behavior is shown in Figure 2, and is typical for the other M^+(pyridine) complexes. In these cases, the low-energy features for all ions are much smaller than the dominant cross section feature (typically less than 2%), and the two features are quite distinct from one another. Such low-energy features can be attributed either to contamination of the ion beam or to excited states of the M^+(pyridine) species. If the former were true, then we would expect to observe other product ions formed by CID at low energies. No such products were observed except in the case of Cr^+(pyridine). It is possible that a ligand other than pyridine also having a mass of 79 Da might be present, but we can think of no species that should be so weakly bound to metal ions. We therefore believe that these low-energy features can be attributed to electronically excited M^+(pyridine) species. Vibrational and rotational excitation (which should exhibit broad distributions, given the large excitation energies of 1.9−3.0 eV) is excluded by the distinct difference between the low- and high-energy features (Figure 2). Similar features, also attributed to electronic excitation, were previously observed in the CID reactions of M^+(benzene) and M^+(benzene)$_2$ systems.[49]

Threshold Analysis. The model of eq 1 was used to analyze the thresholds for reactions 2 in 12 M^+(pyridine) systems. The presence of the low-energy features in many of the systems complicates the data analysis. In each case, the data are analyzed before and after subtraction of the low-energy feature (also analyzed using eq 1 with internal energies but no lifetime effect included). The reported values represent the average values determined. The variations in the measured thresholds are included in the uncertainties reported. The results of these analyses are provided in Table 1 for all 12 metal ions and representative results are shown in Figure 3 for the Fe^+(pyridine) complex. In all cases, the experimental cross sections for reactions 2 are accurately reproduced using a loose PSL TS model.[4] Previous work has shown that this model provides the most accurate assessment of the kinetic shifts for CID processes

(48) Meyer, F.; Khan, F. A.; Armentrout, P. B. *J. Am. Chem. Soc.* **1995**, *117*, 9740.

(49) Meyer, F.; Khan, F. A.; Armentrout, P. B. *J. Am. Chem. Soc.* **1995**, *117*, 9740.

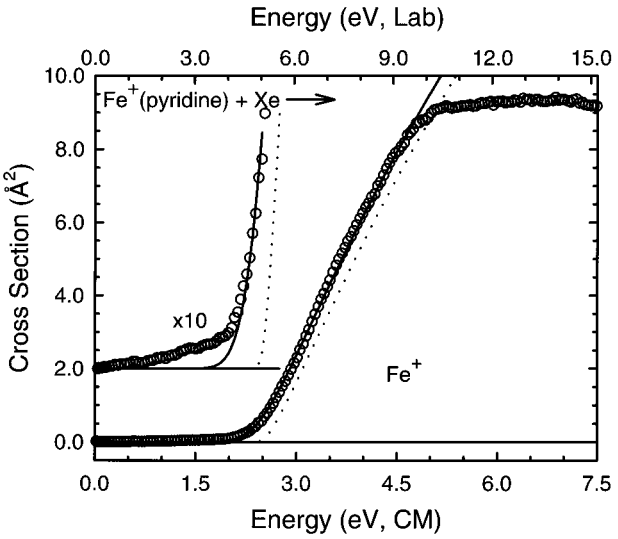

Figure 3. Zero pressure extrapolated cross section for collision-induced dissociation of the Fe^+(pyridine) complex with Xe in the threshold region as a function of kinetic energy in the center-of-mass frame (lower *x*-axis) and the laboratory frame (upper *x*-axis). (Note: The low-energy feature has not been subtracted.) A solid line shows the best fit to the data using eq 1 convoluted over the neutral and ion kinetic energy distributions. A dashed line shows the model cross sections in the absence of experimental kinetic energy broadening for reactants with an internal energy corresponding to 0 K.

for electrostatic ion−molecule complexes.[2−4,43,44] Good reproduction of the data is obtained over energy ranges exceeding 3.5 eV and cross section magnitudes of at least a factor of 100. Table 1 also includes values of E_0 obtained without including the RRKM lifetime analysis. Comparison of these values with the E_0(PSL) values shows that the kinetic shifts observed for these systems vary from 0.10 to 0.30 eV. The total number of vibrations, 30, and heavy atoms, 7, remains the same in all of these M^+(pyridine) complexes and hence the number of low-frequency vibrations remains the same. This implies that the observed kinetic shift should directly correlate with the density of states of the complex at threshold, which depends on the measured BDE. This is exactly what is found, as shown in Table 1.

The entropy of activation, $\Delta S^\dagger$, is a measure of the looseness of the TS and also a reflection of the complexity of the system. It is largely determined by the molecular parameters used to model the energized molecule and the TS, but also depends on the threshold energy. Listed in Table 1, $\Delta S^\dagger$(PSL) values at 1000 K show little variation, as expected based upon the similarity of these systems, and range between 32 and 40 J mol^{-1} K^{-1} across these systems. These entropies of activation can be favorably compared to $\Delta S^\dagger_{1000}$ values in the range of 29−46 J K^{-1} mol^{-1} collected by Lifshitz for several simple bond cleavage dissociations of ions.[50]

Theoretical Results

Theoretical structures for neutral pyridine and for the complexes of pyridine with Mg^+, Al^+, Sc^+, Ti^+, V^+, Cr^+, Mn^+, Fe^+, Co^+, Ni^+, Cu^+, and Zn^+ were calculated as described above. Table S3 gives details of the final geometries for each of these species. Results for the most stable conformation of the Fe^+(pyridine) complex are shown in Figure 4.[51]

(50) Lifshitz, C. *Adv. Mass Spectrom.* **1989**, *11*, 113.

(51) Figures were generated using the output of Gaussian98 geometry optimizations in the Hyperchem Computational Chemistry Software Package, Version 5.0, Hypercube Inc., 1997.

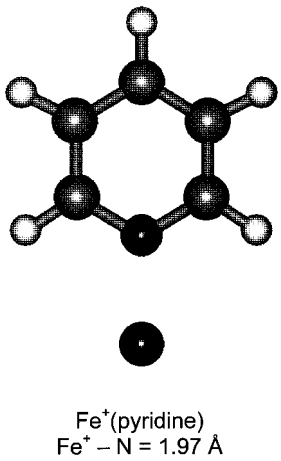

Figure 4. Optimized B3LYP/6-31G(d,p) geometry of Fe^+(pyridine).

Table 2. Enthalpies and Free Energies of Metal Ion Binding of M^+−Pyridine at 298 K (in kJ/mol)[a]

M^+	ΔH_0	$\Delta H_{298} - \Delta H_0$[b]	ΔH_{298}	$T\Delta S_{298}$[b]	ΔG_{298}
Mg^+	200.0(6.4)	1.3(0.2)	201.3(6.4)	30.5(0.7)	170.8(6.4)
Al^+	190.3(10.3)	1.2(0.2)	191.5(10.3)	30.4(0.7)	161.1(10.3)
Sc^+	231.5(10.3)	0.9(0.2)	232.4(10.3)	29.8(0.7)	202.6(10.3)
Ti^+	217.2(9.3)	1.2(0.2)	218.4(9.3)	31.1(0.7)	187.3(9.3)
V^+	218.7(13.5)	1.4(0.2)	220.1(13.5)	31.9(0.7)	188.2(13.5)
Cr^+	197.1(11.3)	1.3(0.2)	198.4(11.3)	31.9(0.7)	166.5(11.3)
Mn^+	181.7(8.6)	0.9(0.2)	182.6(8.6)	30.2(0.7)	152.4(8.6)
Fe^+	223.7(8.9)	1.3(0.2)	225.0(8.9)	31.7(0.7)	193.3(8.9)
Co^+	246.8(12.3)	1.5(0.1)	248.3(12.3)	32.7(0.4)	215.6(12.3)
Ni^+	254.8(15.2)	1.7(0.2)	256.5(15.2)	33.3(0.7)	223.2(15.2)
Cu^+	245.9(10.1)	1.6(0.2)	247.5(10.1)	33.2(0.7)	214.3(10.1)
Zn^+	246.9(6.9)	1.2(0.2)	248.1(6.9)	31.7(0.7)	216.4(6.9)

[a] Uncertainties are listed in parentheses. [b] Density functional theory values from calculations at the B3LYP/6-31G(d,p) level of theory with frequencies scaled by 0.9613.

Not surprisingly, the calculations find that the metal ion prefers to be bound to the nitrogen atom rather than the π cloud of the aromatic ring of pyridine. Attempts were made to calculate stable π-complex geometries, but the starting π-complex geometries always converged to the energetically more favorable planar geometry. This indicates that the σ interaction with the lone pair of electrons on the nitrogen atom is indeed stronger than that with the π cloud. Overall, we conclude that there is only a single stable geometry for the M^+(pyridine) complexes. Further, because of the strong ion−dipole and ion−induced dipole interactions, the potential energy surface for M^+ + pyridine should be attractive such that there are no barriers in excess of the bond energy for dissociation of M^+(pyridine). In general, the distortion of the pyridine molecule that occurs upon complexation to a metal ion is minor, Table S3.

Conversion from 0 to 298 K. To allow comparison to previous literature values and commonly used experimental conditions, we convert the 0 K bond energies determined here to 298 K bond enthalpies and free energies. The enthalpy and entropy conversions are calculated using standard formulas (assuming harmonic oscillator and rigid rotor models) and the vibrational and rotational constants determined for the B3LYP/6-31G(d,p) optimized geometries, which are given in Tables S1 and S2. Table 2 lists 0 and 298 K enthalpy, free energy, and enthalpic and entropic corrections for all systems experimentally determined (from Table 1). Uncertainties in the enthalpic and entropic corrections are determined by 10% variation in the molecular constants. Using these values, we have adjusted enthalpy and free energy values taken from the

Table 3. Experimental and Literature Enthalpies of Proton and Metal Ion Binding to Pyridine at 0 K (in kJ/mol)

	experiment		
reactant	GIBMS[a]	literature[b]	theory
H^+(pyridine)		924.0(16.0)[c]	908.9[e]
Li^+(pyridine)	181.0(14.5)[d]		179.1[e]
Na^+(pyridine)	126.7(2.9)[d]		123.9[e]
K^+(pyridine)	90.3(3.9)[d]		91.1[e]
Mg^+(pyridine)	200.0(6.4)		
Al^+(pyridine)	190.3(10.3)		195.3[f]
Sc^+(pyridine)	231.5(10.3)		
Ti^+(pyridine)	217.2(9.3)		
V^+(pyridine)	218.7 (13.5)		
Cr^+(pyridine)	197.1 (11.3)		
Mn^+(pyridine)	181.7 (8.6)		
Fe^+(pyridine)	223.7 (8.9)	203.7 (11.7)[g]	
Co^+(pyridine)	246.8 (12.3)	249.5 (20.9)[h]	
Ni^+(pyridine)	254.8 (15.2)	249.3 (15.7)[h]	
Cu^+(pyridine)	245.9 (10.1)	274.1 (75.2)[i]	241.8[j]
			274.3[k]
			205.0[l]
Zn^+(pyridine)	246.9 (6.9)		

[a] This work except as noted. [b] All literature values adjusted to 0 K. [c] References 52 and 53. [d] Reference 8. [e] Reference 8, MP2(full)/6-311+G(2d,2p)//MP2(full)/6-31G(d). [f] Reference 22. [g] Reference 17, kinetic method. [h] Reference 18, kinetic method. [i] Reference 19, photodissociation. [j] Reference 19, MP2/[HW(f),6-31G(d,p)]. [k] Reference 19, B3LYP/[HW(f),6-31G(d,p)]. [l] Reference 19, HF/[HW(f),6-31G(d,p)].

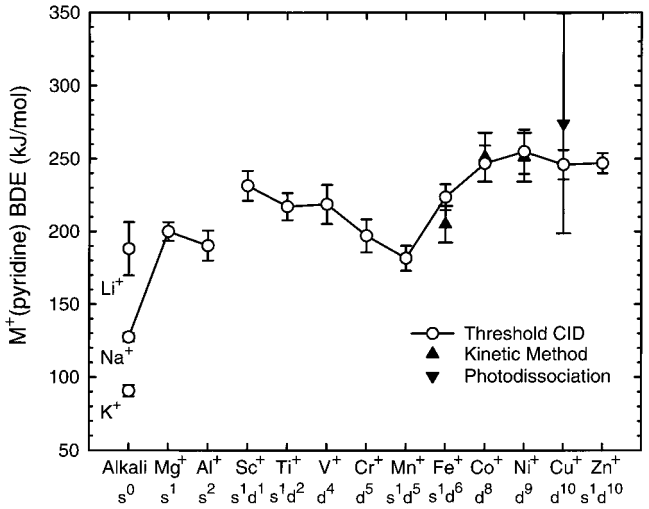

Figure 5. Experimental bond dissociation energies (in kJ/mol) of M^+-EnDash−(pyridine), where $M^+ = Li^+$, Na^+, K^+, Mg^+, Al^+, Sc^+, Ti^+, V^+, Cr^+, Mn^+, Fe^+, Co^+, Ni^+, Cu^+, and Zn^+. All CID values (○) are at 0 K. Experimental results include values from ref 8 (alkali metal ions). Kinetic method (▲, refs 17 and 18) and photodissociation (▼, ref 19) results are also shown. Ground-state electron configurations are provided for each metal ion.

literature[17−19] (listed at 298 K) to 0 K. These are compared to the present results in Table 3 and Figure 5.

Discussion

Comparison of Theory and Experiment. The metal cation affinities of pyridine at 0 K measured here by guided ion beam mass spectrometry are summarized in Table 3. The agreement between calculated bond energies at the B3LYP/6-31G(d,p) level of theory and those determined experimentally is poor and highly dependent upon the d-orbital population. Present results indicate that this level of theory is insufficient to obtain accurate energetics for systems that involve transition metal ions. Theoretical values are not reported here because we believe that the energetic information derived from these calculations is unreliable. This belief is further supported by the inability to properly reproduce ionization energies of the bare transition metals at this level of theory. However, the accuracy of structures and molecular parameters (vibrational frequencies and rotational constants) is not nearly as sensitive to the level of theory employed. Thus, these computational results still allow us to extract accurate thermochemical information from our experimental results. Because we would like to determine what level of theory and basis set size are needed to accurately reproduce binding energies in these and related systems, we are currently pursuing higher level calculations. Preliminary results indicate that increasing the basis set size and including additional diffuse functions (e.g. 6-311+G(2d,2p)) produces almost insignificant changes in calculated geometries and leads to much better agreement with experimental results. These results will be discussed in more detail in a future paper.

Comparison with Theoretical Literature Values. Previous calculations of pyridine have been limited to studies of its interactions with protons,[9,20,21] alkali metal cations,[8] Al^+,[22] Cu^+, and Ag^+.[19] In all of these previous studies, the optimized structures of these complexes are very similar to that found for the complexes examined here with the cation binding to the lone pair electrons on the nitrogen atom. Attempts were also made to calculate stable π-complex geometries, with the alkali metal ions[8] and Al^+,[22] but the starting π-complex geometries always converged to the more energetically favorable planar geometry, as found in this study.

In the previous work, the proton affinity of pyridine was calculated and compared to the experimentally determined value at several levels of theory ranging from semiempirical methods MNDO, INDO, and AM1[21] to ab initio and density functional calculations with varying sized basis sets.[8,9,20,21] The best previous calculations performed are ab initio calculations at the MP2(full)/6-311+G(2d,2p)//MP2(full)/6-31G* level of theory which include both zero point energy corrections (ZPE) and basis set superposition error corrections (BSSE).[8] The proton affinity calculated at this level of theory is 908.9 kJ/mol, 15.1 kJ/mol lower than the experimentally determined value of 924.0 ± 16.0 kJ/mol,[52,53] but it does lie within the somewhat large experimental error in this measurement.

The binding energies of alkali metal ions Li^+, Na^+, and K^+ to pyridine have also been calculated at the MP2(full)/6-311+G-(2d,2p)//MP2(full)/6-31G* level of theory including ZPE and BSSE corrections, and have been experimentally determined by threshold collision-induced dissociation.[8] Much better agreement between the theoretical binding energies determined at this level of theory (179.1, 123.9, and 91.1 kJ/mol) and the experimentally determined values (181.0, 126.7, and 90.3 kJ/mol, respectively) was found. The alkali-metalated complexes are electrostatic in nature with most of the charge localized on the metal center, whereas protonated complexes are more covalent in nature and the charge is highly delocalized. Hence, correlation effects are probably more severe, requiring the use of larger basis sets and higher levels of correlation to achieve accurate enthalpies of protonation.[54] The higher degree of covalency expected in metal−ligand complexes involving transition metal ions suggests that accurate determination of

(52) Meot-Ner, M. *J. Am. Chem. Soc.* **1979**, *101*, 2396.
(53) Hunter, E. P.; Lias, S. G. Proton Affinity Evaluation. In *NIST Chemistry WebBook, NIST Standard Reference Database Number 69*; Mallard, W. G., Lindstrom, P. J., Eds.; National Institute of Standards and Technology: Gaithersburg, MD, November, 1998 (http://webbook.nist.gov.).
(54) Del Bene, J. E.; Shavitt, I. *Int. J. Quantum Chem. Symp. Quantum Chem. Symp.* **1989**, *23*, 445.

binding energies for such systems might also require high levels of correlation to obtain values consistent with the experimental results obtained here.

Yang et al.[19] calculated the Cu^+−pyridine BDE at HF, MP2, and B3LYP levels of theory using several basis sets, the most accurate being HW(f),6-31G(d,p) which employs an effective core potential developed by Hay and Wadt[55] with additional f polarization functions for Cu^+. The calculated 0 K BDE is quite sensitive to the level of theory employed and varied from 206 kJ/mol at the HF level to 242 kJ/mol at the MP2 level of theory, and 274 kJ/mol at the B3LYP level. The HF BDE is obviously much too low (Table 3). The MP2 results are in good agreement with the threshold CID BDE of 245.9 ± 10.1 kJ/mol reported here, while their B3LYP results are somewhat higher. Stöckigt performed calculations on the Al^+(pyridine) system to investigate the out-of-plane motion of the Al^+ ion, moving from the C_{2V} planar geometry to an π-interaction-type geometry.[22] Similar to that observed here, the π-complex geometry was found to be unstable for the pyridine ligand, such that dissociation was the only path observed. On the basis of thermodynamic data reported there, a BDE for Al^+−pyridine of 195.3 kJ/mol is calculated with G2MP2. This value is 5.0 kJ/mol lower than that measured here, Table 3, well within our experimental uncertainty of 10.3 kJ/mol.

Comparison with Experimental Literature Values. Table 3 and Figure 5 also compare the present experimental results to those of Cooks and co-workers,[17,18] used a multi-quadrupole mass spectrometer and the kinetic method to measure the pyridine affinities of several cations. As can easily be seen in the figure, excellent agreement is obtained for the Co^+ and Ni^+ systems. The value they measure for Fe^+ is 20.0 kJ/mol lower than that measured here, but still lies within the combined experimental uncertainties of these two measurements. The difference in the measured Fe^+ may be the result of a spin effect that arises as a result of the difference in the way binding affinities are measured. Cooks and co-workers used benzene as the reference base. Benzene binds to metal ions in a π complex and acts as a 6-electron donor. The Fe^+(pyridine)-(benzene) complex is therefore a 15-electron complex and almost certainly in a quartet state. Adiabatic dissociation of this complex will form Fe^+(benzene) in its quartet ground state, but formation of Fe^+(pyridine) + benzene could occur diabatically, also producing Fe^+(pyridine) in the quartet state. However, if the ground state of Fe^+(pyridine) is a sextet, then the bond energy measured by the kinetic method would be too low by the sextet−quartet excitation energy. As a rough estimate, this excitation energy could be approximately the same as the ^6D−^4F splitting in Fe^+, 22 kJ/mol.[56]

Comparison is also made to the work of Yang et al.[19] In this study, they employed a photodissociation technique in which they were able to derive the Cu^+−pyridine binding energy from the onset of the charge-transfer products, Cu + pyridine$^+$, combined with the ionization energies. The value they derive is somewhat larger than that determined here but well within the large uncertainty in their measurement.

Periodic Trends in the Binding of Metal Ions to Pyridine. In a previous study, the interaction of pyridine with the alkali metal cations was examined.[8] The bond energy is largest for Li^+ and decreases from Na^+ to K^+. This was not unexpected as it can easily be explained based upon simple electrostatic ideas. Alkali metal ions have s^0 electron configurations, and therefore have spherically symmetric electron densities. The metal−ligand bond length is determined primarily by the size of the cation such that the larger the cation radius, the longer the bond length and the weaker the electrostatic interaction, as observed.

The interaction of pyridine with the monocations examined here is not quite as simple as it is for the alkali metal ions. All of the metal ions examined here possess valence electrons. As a result, comparison of trends in the observed binding as the electron configuration is varied allows a systematic evaluation of the influence of the valence electronic structure of the metal ion. In any metal−ligand complex, the bonding between the metal ion and the ligand is dominated by two factors: the ion−dipole electrostatic attraction and the repulsion between the electrons donated to the metal ion and electrons already present. Ligand-to-metal donation and metal-to-ligand back-donation increases the covalent nature of the bond, while retention of electrons promotes ionic character in the bond. The pyridine ligand has three types of orbitals that it can use for bonding at the N atom. The nitrogen lone pair is a donor of electron density, occupied π orbitals may also act as donors of electron density, and the delocalized π^* antibonding orbitals may act as acceptors of electron density.

s Orbital Occupation. Magnesium and aluminum ions have $3s^1$ and $3s^2$ electron configurations, respectively. As the occupation of the s orbital increases, Pauli repulsion between the electron(s) on the metal ion and the nitrogen lone pair increases and it might be expected that the bond energies would also decrease. In contrast, the bond energies are observed to increase from Na^+ to Mg^+ and then to decrease somewhat for Al^+, although it is still more strongly bound than Na^+. The enhancement in the bonding in the Mg^+ and Al^+ systems arises as a result of 3s−3p hybridization.[57−60] Such hybridization polarizes the electron density away from the ligand, which requires energy but exposes a higher nuclear charge to the ligand. In the limit of complete removal of the valence electrons, this would correspond to binding to Mg^{2+} and Al^{3+}. However, electron removal is not complete and sp-hybridization requires more energy for Al^+ than for Mg^+, resulting in less enhancement of the binding in the Al^+ system.

s,d Orbital Occupation. Noncovalent bonds to transition metal monocations are controlled by a balance between ion−dipole attraction and Pauli repulsion between the metal ion and the ligand. Because the ionic radius of the metal decreases from left to right across the periodic table, the electrostatic contribution to bonding also increases. Therefore, the later transition metal ions generally bind more strongly than the early metal ions, as can be seen in Figure 5. Also obvious in the figure is the significant role that s,d orbital occupation plays. All of the first row transition metal ions bind pyridine much more strongly (by at least a factor of 2) than K^+, the $4s^0$ ion of the same periodic row. However, strong variations in the binding across the first row indicate that the binding is influenced by other factors. Such variations have previously been explained for other metal−ligand complexes by examining the electron configuration of each of the metal ions.[61−64] These other factors arise as

(55) Hay, P. J.; Wadt, W. R. *J. Chem. Phys*. **1985**, *82*, 299.
(56) Sugar, J.; Corliss, C. *J. Phys. Chem. Ref. Data* **1985**, *14*, Suppl. 2.
(57) Bauschlicher, C. W., Jr.; Langhoff, S. R.; Partridge, H. *J. Chem. Phys.* **1991**, *94*, 2068.
(58) Bauschlicher, C. W.; Langhoff, S. R.; Partridge, H.; Rice, J. E.; Komornicki, A. *J. Chem. Phys.* **1991**, *95*, 5142.
(59) Bauschlicher, C. W.; Partridge, H. *J. Phys. Chem.* **1991**, *95*, 9694.
(60) Bauschlicher, C. W.; Sodupe, M.; Partridge, H. *J. Chem. Phys.* **1992**, *96*, 4453.
(61) Rosi, M.; Bauschlicher, C. W. *J. Chem. Phys.* **1989**, *90*, 7264.
(62) Rosi, M.; Bauschlicher, C. W. *J. Chem. Phys.* **1990**, *92*, 1876.
(63) Dalleska, N. F.; Honma, K.; Sunderlin, L. S.; Armentrout, P. B. *J. Am. Chem. Soc*. **1994**, *116*, 3519.
(64) Armentrout, P. B. *Acc. Chem. Res*. **1995**, *28*, 430.

a result of the mechanisms by which the transition metal ion is capable of decreasing Pauli repulsion between the metal and the ligand. These mechanisms include 4s−4p polarization, 4s−3dσ hybridization, and promotion to a more favorable electronic state. Because the 4p orbitals lie higher in energy than the 3d orbitals, 4s−4p polarization is more energetic than 4s−3dσ hybridization. 4s−4p polarization is analogous to the mechanism observed in the Mg^+ and Al^+ systems in that it polarizes electron density to the opposite side of the metal ion, away from the ligand, allowing the ligand to experience a larger effective nuclear charge. 4s−3dσ hybridization also hybridizes electron density away from the ligand, but is less energetic and places electron density in a direction perpendicular to the bonding axis. When 4s−3d σ hybridization occurs, the transition metal center exists in a state that is a combination of a $4s^13d^n$ configuration and a $3d^{n+1}$ configuration. Therefore, the promotion energy to the higher lying of these two states must be considered no matter which of these corresponds to the ground state of the metal ion.

Promotion to an electronically excited state is a third mechanism by which Pauli repulsion can be reduced. In the discussion above, 4s−3dσ hybridization involves $3d^{n+1}$ and $4s^1$-$3d^n$ states of the same spin. The thermodynamic consequences of changing spin state to optimize metal−ligand bonding can also be observed, particularly when 4s−3dσ hybridization is not possible (e.g., when $n \geq 5$, there are no $3d^{n+1}$ states of the same spin as high-spin coupled $4s^13d^n$ states). In such cases, promotion to a state of lower spin must occur before 4s−3dσ hybridization can occur. Such promotion becomes more likely as the strength of the ligand field increases. This generally occurs as a result of multiple ligation, which is again not examined here, although pyridine is a stronger field ligand than many of the systems previously examined.

The measured M^+−pyridine BDEs decrease for the early transition metals from Sc^+ to Mn^+. The ground-state electron configuration of Sc^+ is a triplet $4s^13d^1$, and promotion of the ion into a triplet $3d^2$ configuration, emptying the 4s orbital, would decrease the Pauli repulsion, but requires 57.5 kJ/mol.[56] The calculated bond distance, 2.233 Å (Table S3), and charge retained by the metal (0.91e) are the largest of all the transition metal complexes studied.

Ti^+ has two low-lying quartet states; the $3d^3$ configuration is 10.9 kJ/mol higher in energy than the $4s^13d^2$ ground state.[56] The empty 4s orbital of the excited configuration would be the most straightforward acceptor of lone pair electron density, resulting in stronger binding. If the ground state of the Ti^+-(pyridine) complex has appreciable $3d^3$ character, then dissociation to a ground-state $Ti^+(4s^13d^2)$ ion would reduce the apparent BDE by the promotion energy. This possibility is suggested by the observation that the trend in the measured M^+−pyridine BDE would show a monotonic decrease from Sc^+ to Mn^+ if 10.9 kJ/mol were added to the measured BDE of Ti^+(pyridine).

We observe that there is a systematic decrease in the BDE as one moves from Ti^+ to V^+ to Cr^+. Both bare metal ions have high-spin ground states, $3d^4$ and $3d^5$, respectively, with zero occupation of the 4s orbital. With the empty 4s orbital, the primary difference between the two is decreasing ionic radius and consequently increasing charge density, which would predict that Cr^+ would bind more tightly, opposite of that observed. This decrease is most likely the result of the $3d^5$ configuration of Cr^+ forcing occupation of the 3dσ orbital, leading to repulsive interactions with the pyridine ligand.

The Mn^+−pyridine BDE is the weakest of all of the first-row transition metal ions. The low BDE can be attributed to the very stable $4s^13d^5$ electronic configuration of ground-state Mn^+ (^{7}S). Because both the 4s and 3dσ orbitals are occupied and high-spin coupled, the Pauli repulsion between the metal and ligand is the greatest for this complex. The high-spin state of Mn^+ is incapable of 4s−3dσ hybridization without promotion. Such promotion would require a minimum of 113.3 kJ/mol to access the lowest lying quintet electronic state, the ^{5}S ($4s^13d^5$) state.[56] As a result, the charge retained by the metal and the metal−ligand bond distance is quite large. Of the transition metal ions, only Sc^+ retains more charge and has a longer metal−ligand bond length.

The M^+−pyridine BDE increases for the late transition metal ions starting from Fe^+, reaching a maximum for Ni^+, and falling off slightly for Cu^+ and Zn^+. The ground-state electron configurations of the Co^+, Ni^+, and Cu^+ ions have $3d^n$ populations. This allows for direct donation of the electron pair into the empty 4s orbital of the metal ion. Further, the size of the metal ion decreases with increasing d orbital population resulting in stronger binding. The decrease in BDE from Ni^+ to Cu^+ most likely results from an increased occupation of the 3dσ orbital, similar to that observed for V^+ vs Cr^+.

Iron ion has an excited state, ^{4}F, that lies only 22.4 kJ/mol above the ^{6}D ground state.[56] The excited state has an $3d^7$ configuration that should decrease the Pauli repulsion between the metal and the pyridine ligand. The Fe^+ bond energy is just about 22 kJ/mol weaker than the Co^+ bond energy. The relative bond energies are very comparable to those observed for ammonia complexes by Walter and Armentrout.[65] The weaker bond is consistent with either a sextet ground state (weaker because of the 4s orbital occupation) or a quartet ground state (weaker because it dissociates adiabatically to the Fe^+(^{6}D), 22 kJ/mol lower than the diabatic asymptote).

Copper ion has a $3d^{10}$ configuration and its BDE is consistent with the other late transition metals. However, the decrease in ionic radius upon filling the d shell should increase the charge density and strengthen the ion−dipole interaction. This is supported by calculations that find that the Cu^+−pyridine bond length is the smallest of all systems studied here.

The electron configuration of Zn^+ is $4s^13d^{10}$. Occupation of the 4s orbital results in an increase in Pauli repulsion, yet the measured BDEs to Cu^+ and Zn^+ are equal to within experimental error. The effect is much smaller (and appears to be within the experimental uncertainties of these measurements) than that observed for Mn^+ as a result of the much smaller size and consequently higher charge density of Zn^+.

Comparison to Other Ligands. Collision-induced dissociation studies have been made of transition metal complexes with ammonia,[65] water,[29] carbonyl,[30,31,66] ethene,[67] and benzene[45] ligands. The binding energies of ammonia and water show trends similar to that observed here for pyridine. The behavior observed with benzene, carbonyl, and ethene ligands is somewhat different. Figure 6 compares the trends in the M^+−pyridine BDEs measured here to those previously measured for the ligands mentioned above.

The bond between the metal ion and the ligand consists of ligand-to-metal σ electron density and π electron density. The relative ease with which a metal ion can accept electron density

(65) Walter, D.; Armentrout, P. B. *J. Am. Chem. Soc.* **1998**, *120*, 3176.

(66) Sievers, M. R.; Armentrout, P. B. *J. Phys. Chem.* **1995**, *99*, 8135. Schultz, R. H.; Crellin, K. C.; Armentrout, P. B. *J. Am. Chem. Soc.* **1991**, *113*, 8590. Goebel, S.; Haynes, C. L.; Khan, F. A.; Armentrout, P. B. *J. Am. Chem. Soc.* **1995**, *117*, 6994. Khan, F. A.; Steele, D. A.; Armentrout, P. B. *J. Phys. Chem.* **1995**, *99*, 7819. Meyer, F.; Chen, Y.-M.; Armentrout, P. B. *J. Am. Chem. Soc.* **1995**, *117*, 4071.

(67) Sievers, M. R.; Jarvis, L. M.; Armentrout, P. B. *J. Am. Chem. Soc.* **1998**, *120*, 1891.

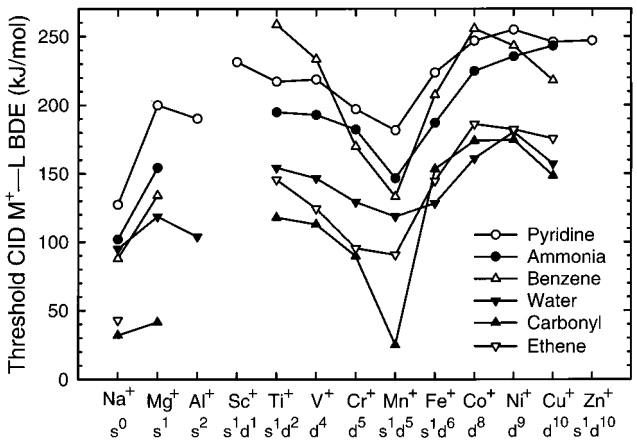

Figure 6. Comparison of the periodic trends in the M^+-L bond dissociation energies determined by collision-induced dissociation. Ligands, L, include pyridine (○), ammonia (●), benzene (△), carbonyl (▲), ethene (▽), and water (▼). Values are taken from present work and refs 8, 29, 30, 31, 45, 64, 65, and 66. Ground-state electron configurations are provided for each metal ion.

changes relatively little with the ligand, but is strongest when the donor and acceptor orbitals lie closest in energy, or when more than two electrons are donated as in benzene. However, the ease of additional ligand-to-metal donation (π donor) or metal-to-ligand back-donation (π acceptor) interaction depends on both the ligand and the d-orbital population of the metal ion. If all other factors (charge density and electron polarizability of the metal ion, and dipole moment and polarizability of the ligand) are the same, then the trend in binding energies will be controlled by the d-orbital population of the metal ion and the π donor/acceptor behavior of the ligand. For the early transition metals, with partially occupied d orbitals, binding to ligands capable of both σ and π donation is enhanced relative to that of σ donor, or σ donor and π acceptor ligands. For the late transition metals with high d-orbital occupation, a greater enhancement in binding is expected for π-acceptor ligands, over σ and π donor, and σ donor ligands.

Ammonia is a σ donor, water is both a σ and π donor, carbonyl and ethene are σ donors and π acceptors, while benzene is a π donor and π acceptor ligand. On the basis of a comparison to these ligands, considering both symmetry and energy arguments, pyridine may participate in all three types of interactions. A σ donation interaction arises from donation of electron density from the pyridine $11A_1$ orbital, which is essentially the lone pair on the nitrogen atom of the ligand. A π donation interaction could involve the $2B_1$ π bonding orbital that is heavily localized on the nitrogen atom and the carbon atom para to it. A π acceptor interaction should be possible by donation of electron density from the metal d orbitals into the $3B_1$ π^* antibonding orbital, which is also heavily localized on the nitrogen atom and the carbon atom para to it. Indeed this orbital is calculated to be more stable (lower in energy) than the π* acceptor orbitals on known π acceptor ligands, CO, ethene, and benzene.[68] However, CO can accept π electron density in two orthogonal orbitals that are only slightly less stable than that in pyridine and these orbitals are more highly localized than those in pyridine and thus CO should exhibit the strongest π acceptor behavior. It is therefore conceivable that the trends in the M^+-pyridine BDEs might parallel any of these ligands. The trends observed in the M^+-ligand BDEs to the early transition metal ions are similar for all ligands except benzene, although pyridine most closely parallels that of ammonia and water. The largest deviations in behavior are observed for Mn^+ and the late transition metal ions. For all ligands, the Mn^+-ligand BDE is the lowest measured of all of the transition metal ions. However, water does not show a highly pronounced dip for Mn^+, as all the other ligands do. For the late metals, the carbonyl and water trends parallel the pyridine in all respects, while ammonia, benzene, and ethene fail to track the peak in BDE for Ni^+ and decline for Cu^+.

In their study of the binding of transition metal ions to ammonia, Walter and Armentrout[65] noted distinct differences in the average percent increase observed in bonding from the early to the late transition metal ions depending on whether the ligand was a π donor, π acceptor, or neither. Relative to ammonia, which shows a 32% increase associated primarily with the relative sizes of the metal ions, water is a π donor and shows only a 16% increase. A much larger increase of 60% was observed for CO, a π acceptor, as expected based upon the argument above. An 18% increase is measured here for pyridine. (This excludes Sc^+, which was also not included in earlier work; a 15% increase is measured when Sc^+ is included.) This is comparable to that observed for water, indicating that the binding in these pyridine complexes probably results primarily from σ and π donor interactions with no obvious enhancement in binding as a result of the π acceptor interaction. It is a little difficult to understand why the π acceptor interaction is not more important, as the π* antibonding orbitals are slightly lower in energy for pyridine than they are for CO.[68] Hence, the difference in the measured BDEs to ammonia and pyridine (Figure 6) results from the increased polarizability of the ligand and π back-donation in the pyridine complexes. A nearly constant difference in BDE is observed for Ti^+ through Ni^+, a 26 ± 9 kJ/mol increase from ammonia to pyridine. The difference in measured BDE to Cu^+ is much smaller, 9 ± 18 kJ/mol, because Cu^+ cannot accept any π donation from the ligand, whereas all earlier metal ions can. This small difference is a rough measure of the enhanced binding resulting from the increased polarizability of the pyridine ligand. This suggests that the π donation interaction increases the binding in the pyridine complexes to Ti^+-Ni^+ by 17 ± 20 kJ/mol.

Conclusions

The kinetic energy dependence of the collision-induced dissociation of M^+(pyridine), where $M^+ = Mg^+$, Al^+, Sc^+, Ti^+, V^+, Cr^+, Mn^+, Fe^+, Co^+, Ni^+, Cu^+, and Zn^+, with Xe is examined in a guided ion beam mass spectrometer. The dominant dissociation process in all cases is loss of the intact pyridine ligand. Thresholds for these processes are determined after consideration of the effects of reactant internal energy, multiple collisions with Xe, and lifetime effects (using methodology described in detail elsewhere).[4] Insight into the structures and binding of the metal ions to pyridine is provided by density functional theory calculations of these complexes performed at the B3LYP/6-31G(d,p) level of theory. Theoretical calculations with such a small basis set are unable to reproduce the trends observed in the experimentally determined BDEs. However, the accuracy of structures and molecular parameters (vibrational frequencies and rotational constants) should be adequate for use in extracting accurate thermochemical information from our experimental results. The trends in measured BDEs may be explained by examining the electron population of the valence orbitals on the metal ion such that binding is the strongest for ions with d^n-type configurations. Further, binding is strongest when the d orbitals are nearly full, primarily a result

(68) Jorgensen, W. L.; Salem, L. *The Organic Chemist's book of Orbitals*; Academic Press: New York, 1973.

of the decreasing size of the metal ion with increasing nuclear charge and of π back-donation. Periodic trends in the M^+−pyridine BDEs are similar to those seen for ligands with similar binding modes and most closely parallel those observed for ammonia ligands.

Acknowledgment. We thank P. B. Armentrout for allowing us to use the guided ion beam mass spectrometer with which these experiments were conducted. This work was supported in part by an ASMS Research Award from Micromass.

Supporting Information Available: Tables of vibrational frequencies and average vibrational energies, rotational constants, and B3LYP/6-31G(d,p) geometry optimized structures of neutral and metalated pyridine and figures showing cross sections for the collision-induced dissociation of M^+(pyrdine) complexes (PDF). This material is available free of charge via the Internet at http://pubs.acs.org.

JA0027923